Supplementary Information

This section provides supporting information for article "Dynamic weakening by nanoscale smoothing during high velocity fault slip" by Xiaofeng Chen et al. Figures in the paper are mentioned by their original number, and figures&Tables that appear only here are labeled as 'Fig. DR#' and 'Table DR#'. Supporting references are listed in the end of this document.

The topics covered here are:

1. Experimental setup including sample composition and macroscopic friction results.
2. Modes of usage of the Atomic Force Microscope (AFM), focusing on measuring friction in the glass-bead method and the relevant calculations. The friction data in the paper were determined in this method.
3. AFM friction measurements: procedures, results and stress calculations Nano-morphology methods and calculations of power-spectral-density (PSD) and surface roughness.
4. Additional references

ROCK-FRICTION EXPERIMENTS

ROCK SAMPLES

Sierra White granite. The electron-microprobe (EMP) modal analysis shows six main minerals in this rock: plagioclase (48%), quartz (38%), alkali-feldspar (5%), ferromagnesian- mica (5%), and muscovite (5%). Mean grain size is about 0.3 mm; mean void space in EMP images is ~4%.

Kasota dolomite. The Kasota dolomite were quarried at Mankato, Minnesota, and it is supplied under the commercial name "Kasota valley limestone". The XRD analysis indicates that our samples are 97.3% dolomite, 2.6% quartz and traces of plagioclase.

HIGH VELOCITY FRICTION EXPERIMENTS

Experimental set-up

The experimental apparatus, called ROGA (Rotary Gouge Apparatus), was built and operated in the University of Oklahoma. It includes three main components: (1) Loading system; (2) Control and monitoring system; and (3) a closed cell to test gouge powder under confined conditions and elevated pore-pressure. ROGA's frame is 1.8 m tall with two decks (Fig. DR1 A-C) that are connected to each other by four internally enforced rectangle legs. The sample (Fig. DR1 D, E) is loaded by a rotary train from below and by the normal stress from above. The power system includes:

(1) A 100 HP three-phase motor and controller that provides constant torque of up to 3,000 Nm from 0 RPM to 3300 RPM. The motor velocity is monitored and controlled through an 8192 sector encoder.
(2) A 225 kg flywheel to boost motor torque; it is engaged with a pneumatic clutch.
(3) An electro-magnetic large clutch that is capable of full engagement in 30 ms.
(4) A hydraulic piston system with axial load up to 9,500 N.

Control and monitoring system

The control and monitoring system is based on National Instruments components, and it includes a SCXI-1100 with modules 1124 (analog control) 1161 (relay control), 1520 (load cell/strain gage), and 1600 (data acquisition and multiplexer), as well as a USB-6210 (encoder measurements). We use LabView and main control software. Digital sampling rate is up to 10 kHz. Load-cells for axial load and

torque are made by Honeywell, gouge dilation/compaction is measured with four eddy-current sensors (about 1 micron accuracy), temperature measurement is with thermo-couples, and sample velocity is monitored by an encoder.

Sample preparation

The experiments were conducted on bare, solid blocks of Sierra White granite and Kasota dolomite. Each sample includes two cylindrical blocks of 101.6 mm diameter and 50.8 mm height. The upper block has a raised ring structure with inner diameter of 63.2 mm and outer diameter of 82.3 mm (Fig. DR1D, E). The blocks were pressed against each other along the raised ring; velocity at outer diameter is only about 14% higher than the velocity at the inner diameter. The granite blocks are glued by epoxy in aluminum cylindrical holders, surface ground and polished with 600 grit SiC powder. Thermo-couples were cemented into holes drilled 3 mm and 6 mm away from the sliding surfaces (Fig. DR1E).

Experimental procedure

The present experiments on the solid rock blocks were run at room-temperature and room humidity. They were run under controlled, stepped velocity, and the normal stress, σ_n, was kept constant during a given experiment. We used one sample of Sierra White granite, and one sample of Kasota dolomite, and the experimental results are shown here in Fig. DR2A, B.

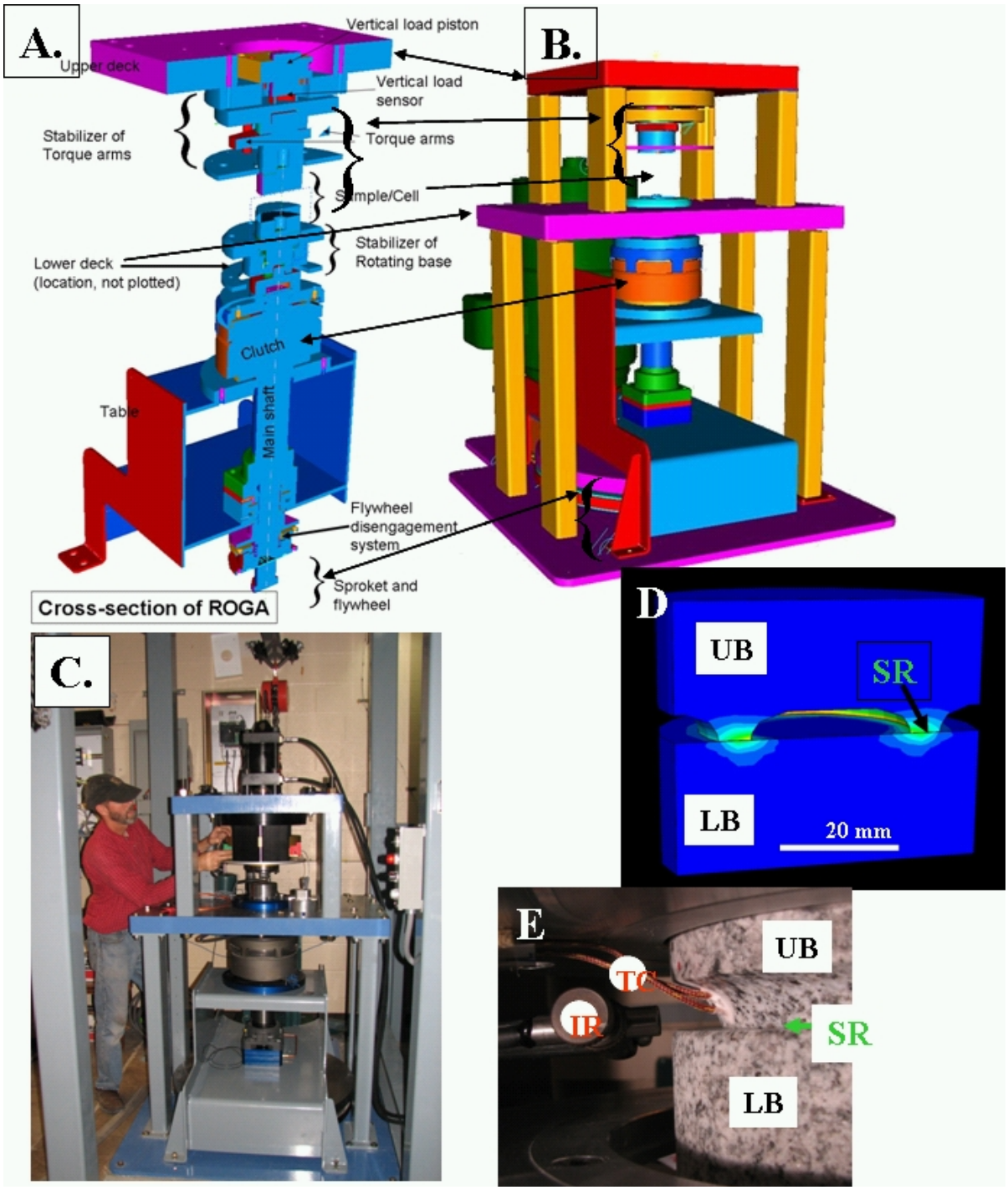

Fig. DR1. The earthquake deformation apparatus. A. Generalized cross section displaying main power train components. B. 3D view of the assembled apparatus. C. View of the system with builder Joel Young. D, E. Blocks of Sierra White granite used in the present experiments. LB-lower block; UB-upper block; SR-sliding ring; TC-thermocouple wires; IR-infra red sensor; EG-gouge ejected from the sliding ring. D.A vertical cut-through the blocks in a finite-element model showing model geometry and temperature distribution due to frictional heating. E. Sample blocks assembled in the loading frame; note two thermocouple wires cemented into the sliding ring.

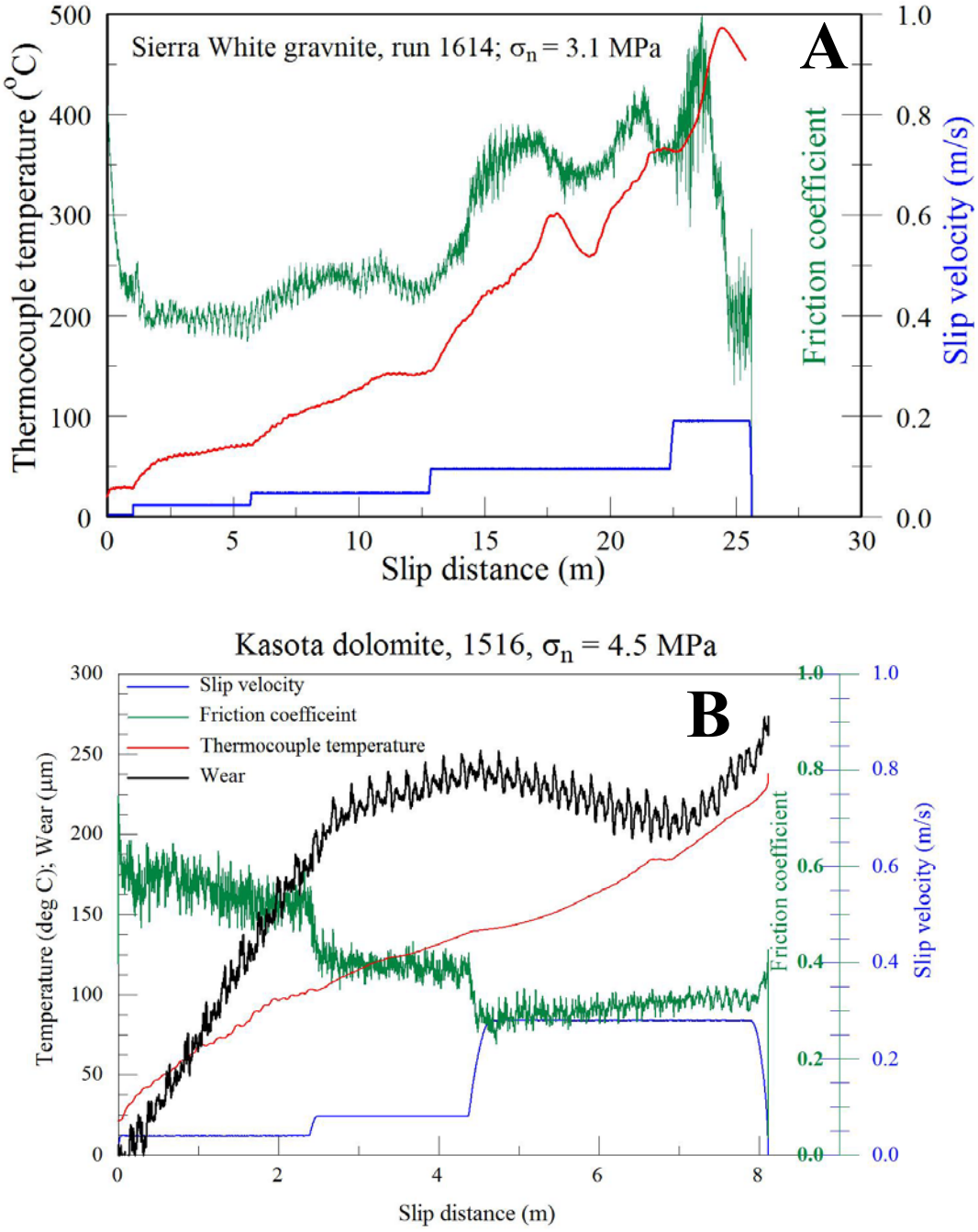

Fig. DR2. (A) velocity loading history and corresponding friction and temperature for Sierra White granite run 1614. (B) velocity, friction, temperature, and wear data for Kasota dolomite, run 1516.

ATOMIC FORCE MICROSCOPE UTILIZATION

AFM MODES

We used two modes of AFM operation. The micro/nanoscale topography of the fault surfaces was imaged with a *Pacific Nanotechnology Nano R2* AFM using the standard 'close contact' imaging mode (also called non-contact or tapping mode, depending on whether the tip penetrates the absorbed water layer). In this mode the cantilever oscillates at a frequency close to its resonant frequency while the tip interaction forces modify the cantilever oscillation frequency and hence its amplitude. This modification of the resonant frequency is combined with a feedback loop system that maintains a constant oscillation amplitude or frequency by adjusting the average tip-to-sample distance. The tip-to-sample distances are recorded at each point (x, y) to construct the topographic image. The common probe used for imaging has a sharp tip with radius of curvature 10~100 nm mounted on the end of a flexible cantilever and tip motion resolution of less than 1 nm, and cantilever force resolution of less than 1 nN were obtained.

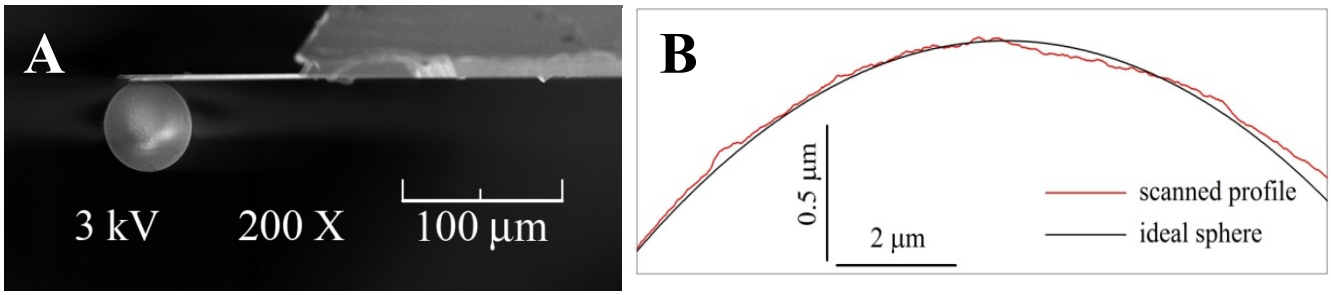

Fig. DR3. A: An SEM image of the fabricated glass-bead probe for our Nano R2 AFM platform. The glass-bead diameter is 50 µm and the cantilever length is 100 µm. B: 1D AFM profile of the glass-bead (red) compared to ideal sphere shape (black); note asperities and roughness at submicron scale.

For the measurement of the friction coefficient we closely followed a recently developed AFM method (Stiernstedt et al. 2005; Attard et al. 2007) in which a spherical glass-bead (10s of microns diameter) replaces the sharp tip on the cantilever (Fig. DR3A). The cantilever with the glass-bead is moved vertically to approach and retract with respect to the sample surfaces (Fig. DR4). The force-distance curves of the interaction forces during this motion are presented by the deflection voltage versus z-piezo displacement curves (Fig. DR4), where deflection voltage records the displacement of a laser beam in a position-sensitive detector reflected from the back of the flexible cantilever. The deflection voltage is proportional to force, considering the cantilever spring constant. The cantilever with the glass-bead is inclined with respect to the sample surface (Fig. DR4), and this inclination generates frictional slip at the contact area between the glass-bead and sample surface (red arrows in Fig. DR4). The friction force inverses its sense during the shift from approaching to retraction according to the change of sliding between glass-bead and sample surface. This sense inversion of the frictional force changes the deflection of the cantilever since the torque applied on the cantilever changes. The result is a force-distance curve with hysteresis between approaching and retracting lines (Fig. SDR4). The analysis of the slopes of the force-distance curves with hysteresis can be combined with geometric and mechanical parameters of the cantilever to calculate the friction coefficient as shown below and elsewhere (Stiernstedt et al. 2005).

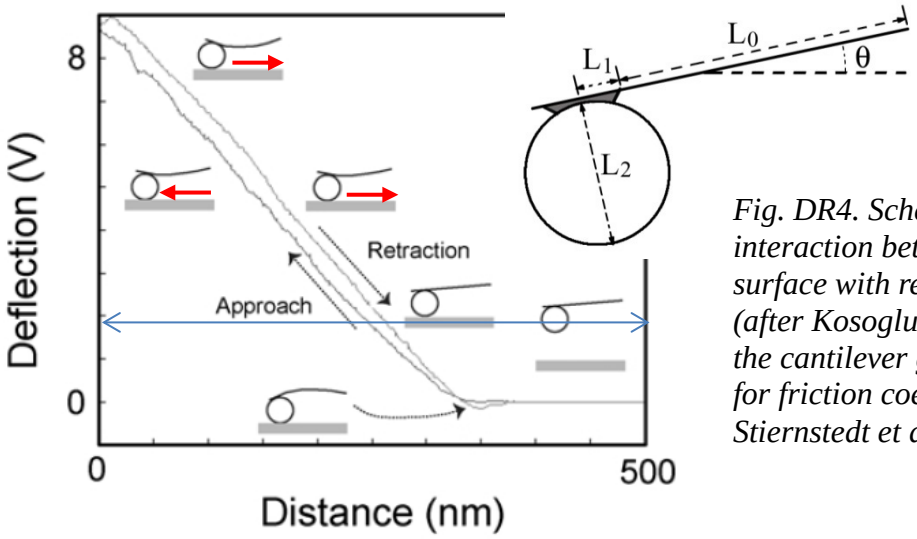

Fig. DR4. Schematic illustration of the interaction between glass bead and sample surface with respect to the force curve (after Kosoglu et al. 2010). Inset displays the cantilever geometric parameters needed for friction coefficient calculations(after Stiernstedt et al. 2005).

FRICTION MEASUREMENT PROCEDURE

Glass-bead probe fabrication

The glass-bead probe preparation is of central importance for successful friction measurements. We followed the procedure of Kosoglu et al. 2010. To fabricate the probes, we used: (1) rectangular, tip-less Silicon AFM cantilevers with aluminum backside coating from *Mikromasch*; (2) silicon oxide microspheres of ~50 micron diameter from *Microspheres-Nanospheres;* and (3) *Loctite* marine epoxy. The *Nano-R2* system has an optic microscope and x-y-z piezo controller, which make it excellent platform for assembling the microsphere onto the end of the cantilever.

Glass-beads were cleaned in de-ionized water and ultrasonically vibrated for a few minutes to remove potential adhesive particles. Then, glass-bead was dropped onto a clean mica surface and dried by heating the mica on a hotplate. The cantilever end was slowly moved down into a tiny drop of epoxy, gently raised up, placed above the glass bead, and then moved down into contact with the top of the glass-bead. Once contact was made, the cantilever with the glued glass-bead was slowly raised, and left undisturbed to cure for 24 hours.

During the fabrication process, glue contamination was avoided on the glass-bead and the backside of the cantilever. Glue contamination on the bead, especially the contact area, may lead to non-direct contact between the glass-bead and the sample surface, and contamination on the back side of the cantilever may lead to reduced optical reflective signal. The fabricated probe was imaged with a Scanning Electron Microscope (SEM) (Fig. DR3A) to determine the cantilever geometry for the friction coefficient calculations and to inspect the glue quality.

Force-distance curve analysis

The force-distance curves for the friction coefficient analysis were determined with a *Veeco Dimension 3100* AFM at Brigham Young University. Under the force-curve mode, this AFM can collect repeating force curve data automatically at the same spot, either in air or under solution that covers the sample and tip by a meniscus. The operator controls the ramp size (the z piezo movement distance) and repeating frequency that in turn controls the bead sliding velocity and the size of the contact region.

Prior to rock friction measurements, the fabricated probe was applied to fresh-cleaved biotite surfaces. The extracted friction coefficient was compared to reported values to ensure the accuracy of this method. The glass bead method yielded an friction coefficient of 0.27±0.01 (Attard et al. 2007),

0.29±0.03 (Attard et al. 2007), 0.29±0.02 (Kosoglu et al. 2010) on wet mica as reported; and our friction coefficient is 0.27±0.02, which agreed well with literature.

Before the rock friction measurement, the glass-bead probe and the rock surfaces were cleaned in a UV-Ozone cleaner for 20 min. The force-distance curve measurements were conducted either parallel or normal the slickensides striations by aligning the cantilever long axis in the selected direction. Once positioned, preliminary curves were obtained to observe the quality of the force-distance curves. A good curve has the following properties (Fig. DR5): (1) zero line at large separation; (2) constant compliance line in the contact region; and (3) clear hysteresis between the approaching and retracting curves (Fig. DR4, DR5). If these properties were satisfied, we then collected force curve data at that position with hundreds of repetitions.

Calculation of the friction coefficient

The detailed derivation of the friction coefficient calculation was presented by Stiernstedt et al. 2005. The required parameters are the probe geometry (including total length of the cantilever, length of the flexible part of the cantilever L_0, length of the glue spot L_1, diameter of the sphere L_2, and inclination angle of the cantilever θ) as well as the slopes of the most linear part of the compliance region from the force curve hysteresis (Fig. DR4). In our case, the probe geometry parameters are cantilever total length 130 μm, glue spot length 10 μm, cantilever flexible part length 100 μm, sphere diameter 50 μm, and cantilever inclination of 12° (Fig. DR3). Calculations were conducted with Matlab.

FRICTION COEFFICIENT DATA

NANO-FRICTION MEASUREMENTS IN THE GLASS-BEAD METHOD

We measure and calculated the friction coefficients in 18 positions in which we had 43 sites, and in each we had tens to hundreds of repeat measurements. Table DR1 below summarizes the results for all this sites and Table DR2 list the average friction coefficients according to rock type, orientation (parallel and normal to slickensides) and conditions (room-dry or wet). The data of Table DR2 is used in Figs. 2 and 3 of the paper.

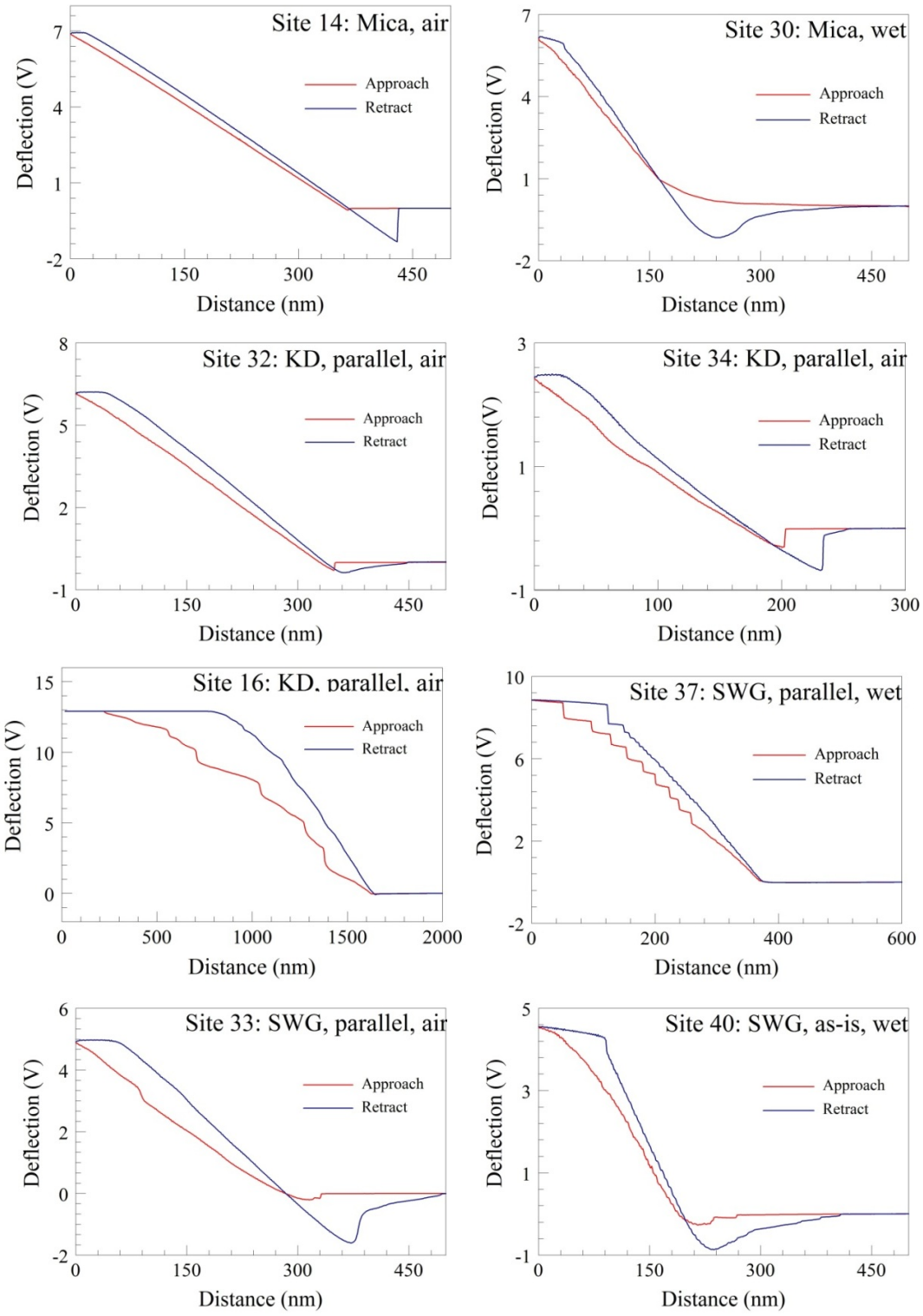

Fig. DR5. Representative force curves of the AFM friction measurement method.

Table DR1. Summary of AFM friction measurements

Site #	Rock type	Surface orientation	Condition	Ramp (μm)	# of repeat	Friction coeff. (Mean ± Stdev)		Comments
						each data point	group of data points	
16	KD	parallel	room-dry	0.5 2 3	133 69 207	0.43 ± 0.096 0.63 ± 0.033 0.64 ± 0.041	0.34±0.17 (8)	Stick-slip? Stick-slip?
31	KD	parallel	room-dry	2	35	0.67 ± 0.051		low quality
32	KD	parallel	room-dry	0.5 1.5	38 35	0.364 ± 0.056 0.295 ± 0.013		
34	KD	parallel	room-dry	0.3	67	0.26 ± 0.043		
32-1	KD	parallel	wet	0.1 0.2 0.4 0.6	113 60 60 99	0.23 ± 0.035 0.17 ± 0.044 0.092 ± 0.05 0.13 ± 0.043	0.15±0.05 (5)	Unstable
34-1	KD	parallel	wet	0.3	76	0.12 ± 0.029		
36	KD	normal	wet	0.15 1	44 41	0.14 ± 0.035 0.277 ± 0.023	0.21±0.1 (2)	
19	KD	normal	room-dry	0.5 2	57 44	0.56 ± 0.018 0.67 ± 0.015	0.56±0.12 (5)	
20	KD	normal	room-dry	0.3 0.5 1.5	38 53 53	0.63 ± 0.01 0.571 ± 0.023 0.37 ± 0.024		Middle linear part Middle linear part Middle linear part
21	KD	As-is	room-dry	0.4 3	35 47	0.54 ± 0.121 0.685 ± 0.034	0.61±0.1 (2)	
33	SWG	parallel	room-dry	0.3 0.5	56 29	0.503 ± 0.022 0.545 ± 0.023	0.52±0.03 (2)	
37	SWG	parallel	wet	0.2 0.3 0.4 0.6 1 3	13 7 4 84 37 34	0.279 ± 0.033 0.3 ± 0.022 0.36 ± 0.026 0.338 ± 0.029 0.296 ± 0.021 0.43 ± 0.028	0.33±0.06 (6)	part of linear region part of linear region part of linear region Stick-slip? Stick-slip?
22	SWG	rough	room-dry	0.5 2	60 42	0.73 ± 0.003 0.7 ± 0.009	0.72±0.02 (2)	
23	SWG	As-is	room-dry	0.3 1 3 5	31 34 49 24	0.61 ± 0.016 0.62 ± 0.011 0.71 ± 0.037 0.625 ± 0.014	0.64±0.05 (4)	
40	SWG	As-is	wet	0.3 0.5 1	76 43 28	0.397 ± 0.03 0.45 ± 0.032 0.394 ± 0.018	0.41±0.03 (3)	
14	biotite	fresh-cleave	room-dry	0.5	102	0.15 ± 0.024	0.15±0.01 (2)	
15	biotite	fresh-cleave	room-dry	0.5	102	0.14 ± 0.008		
30	biotite	fresh-cleave	wet	0.4 0.5 1	33 39 44	0.26 ± 0.043 0.29 ± 0.037 0.26 ± 0.034	0.27±0.02 (3)	

Table DR2. Friction coefficient results in AFM measurements

Rock type	Friction coeff. (Mean ± Stdev)	Test conditions						
		Parallel		Normal		As-is		Rough
		dry	wet	dry	wet	dry	wet	dry
KD	data points	8	5	5	2	2	NA	NA
	μ	0.34±0.17	0.15±0.05	0.56±0.12	0.21±0.1	0.61±0.1		
SWG	data points	2	6	NA	NA	4	3	2
	μ	0.52±0.03	0.33±0.06			0.64±0.05	0.41±0.03	0.72±0.02
Biotite	data points	2				3		
	μ	0.15±0.01 (dry)				0.27±0.02 (wet)		

LOADING STRESSES DURING AFM FRICTION MEASUREMENTS

We apply the Hertz model (Hertz, 1881) to calculate the contact area and the stresses during the glass-bead friction measurements. The normal spring constant of the glass-bead probe was calibrated using the method by Sader et al. 1999, to find a spring constant of 6.5 N/m. The effective spring constant for the cantilever with glass-bead probe is 14.3 N/m by using the scaling factor $(L_{cal}/L_0)^3$. Here L_{cal}=130 μm is the cantilever total length, and L_0=100 μm is the length of the flexible part of the cantilever). This value implies, that a cantilever normal force of 2 μN, the contact area is 0.02~0.07 μm^2 and the normal stress is on the order of a few tens of MPa.

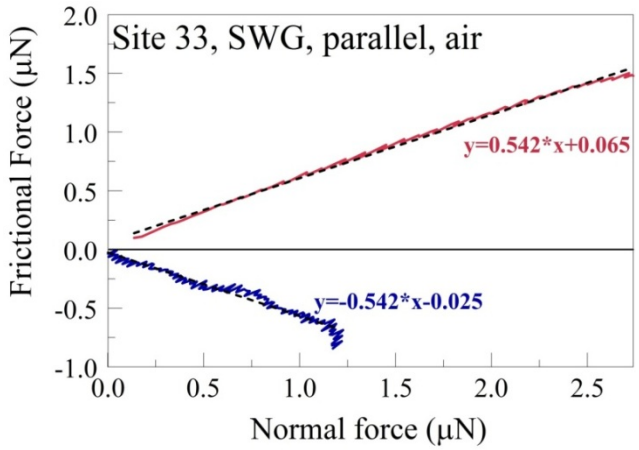

Fig. DR6. Example of normal and frictional force calculations following Stiernstedt et al. 2005. The plot displays the normal force vs. shear force for Site 33, SWG, parallel, room dry.

From the cantilever deflection voltage versus z-piezo displacement curves, we extract normal force versus frictional force curves from the region corresponding to bead-sample contact using the equations in Stiernstedt et al. 2005. Separate linear fits describe the normal versus frictional force trends for the approach and retraction directions (Fig. DR5). The slope of the linear fit line yields the coefficient of friction.

Since the linear fit line to the calculated normal force versus frictional force curves have non-zero intercepts due to adhesion forces which accounts for a significant portion of the total normal force applied at the surface, we shifted the fitted line to cross the zero point and in this way convert the normal force versus frictional force curves to normal stress versus shear stress curves shown in Fig. DR7. The calculated normal and frictional forces are in tens to hundreds of nN, and the friction coefficient values are corresponds to the values we got using the axial glass bead method as described in the main text.

Combining the forces with the contact area calculated from the Hertz model indicate that the normal and shear stress values can reach 50MPa in the present experiments. Stress magnitude here is comparable to crustal stress, raising the possibility to simulate friction process at depth.

NANO-MORPHOLOGY ANALYSIS OF THE FAULT SURFACES

PSD AND ROUGHNESS CALCULATIONS

The AFM topography of the fault surfaces was measured as described above, and some images are presented in Fig. 1. Here we present representative profiles across the fault surfaces (Fig. DR8), and outline the calculations of the power spectral density (PSD). The PSD was calculated from profile data following the method of Sagy and Brodsky, 2009.

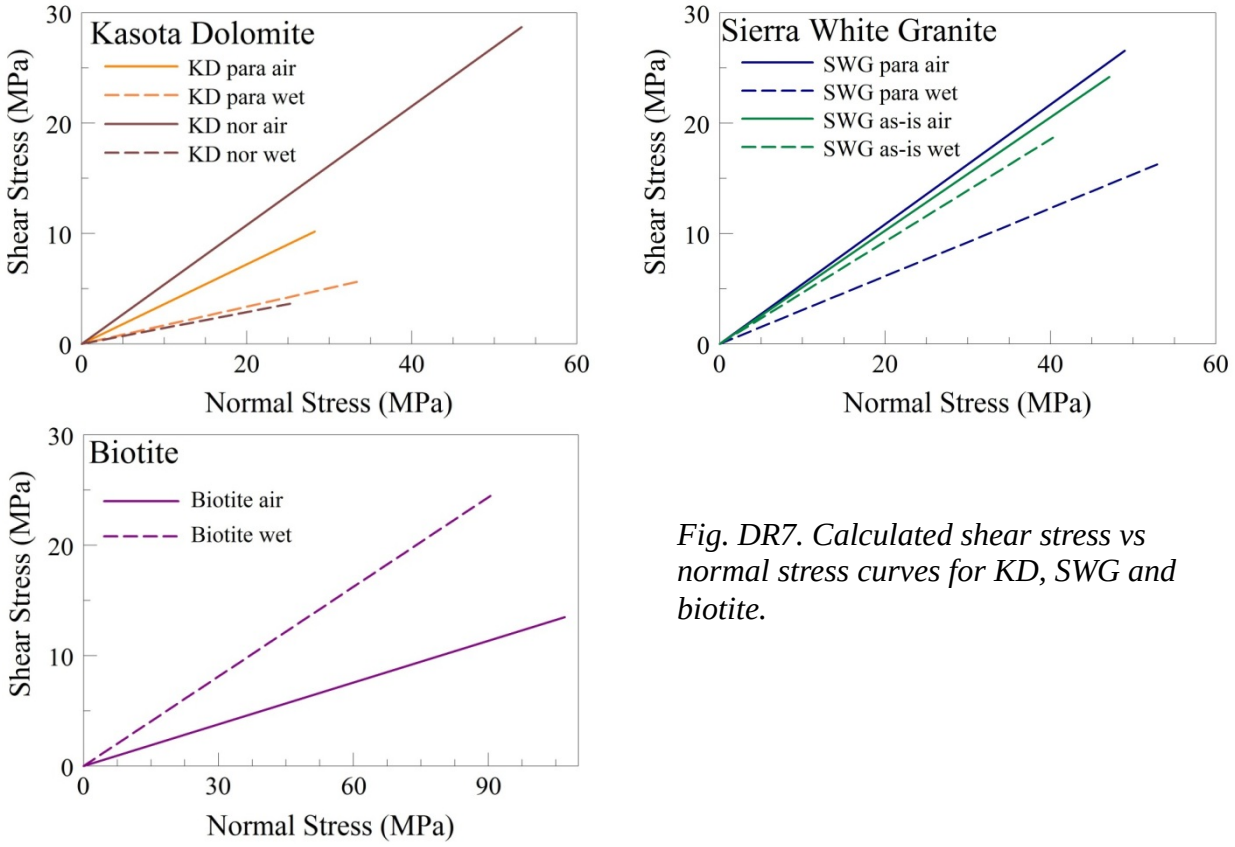

Fig. DR7. Calculated shear stress vs normal stress curves for KD, SWG and biotite.

For each profile $y_i(x)$,

$$(PSD)_i = \frac{\mathcal{F}[y_i(x)]^2 \cdot L}{X^2} \qquad (1)$$

where $\mathcal{F}[y_i(x)]$ is the fast Fourier transform of $y_i(x)$, L is the profile total length, and X is the total number of data points in the profile.

The PSD of the AFM fault surface images was calculated in the following procedure:

1. Extract the digital profile data by drawing lines across the AFM images using the dedicated AFM program *Gwyddion* (http://gwyddion.net/). One example of the extracted profiles was shown in Fig. DR8a, with large amplitude and wavelength differences displayed between profiles parallel and normal to striations.

2. Each set of lines was either parallel- or normal- to the striation lines (Fig. DR8a inset). In each image we selected 50 to 100 individual profiles all at the same length.
3. In *Matlab*, each profile was first leveled by applying the *detrend* command, and the PSD was calculated by using the above equation.
4. The final PSD of an image, for a given orientation is the average PSD of all 50-100 individual profiles. The final PSD curves are plotted in Fig. 3a.

One point should be noted with respect to error presentation in the PSD plot. The data points of the PSD are evenly spaced along the wavenumber ($k = 1/\lambda$) axis, and as the present PSD plot displays wavelength (λ) axis (Fig. 3a), the data points are denser in the shorter wavelength part.

For comparison, synthetic profiles with fixed slope for the PSD plots are also provided as shown in Fig. DR8b. The values for the slopes of the most linear region of the PSD plots are chosen so that the synthetic profiles have the same PSD as the real profiles. Similar amplitude and wavelength characters can be seen fault surface and synthetic profiles.

Roughness values are extracted from the same profile data that we used to calculate the PSD based on their original definition of the roughness parameters. Here the root mean square (RMS) roughness R_q is calculated as the standard deviation of the height differences.

$$R_q = \sqrt{\frac{1}{n}\sum_{i=1}^{n}(y_i - \bar{y})^2} \qquad (2)$$

Since roughness values are scale dependent (Power et al. 1988), relationship between the RMS roughness and profile length can be calculated using Equation (2), by consider averaging the RMS roughness along each profile and the whole profile set data. In the paper, we picked the RMS roughness value at the profile length of 1 μm for KD, SWG, and the glass bead.

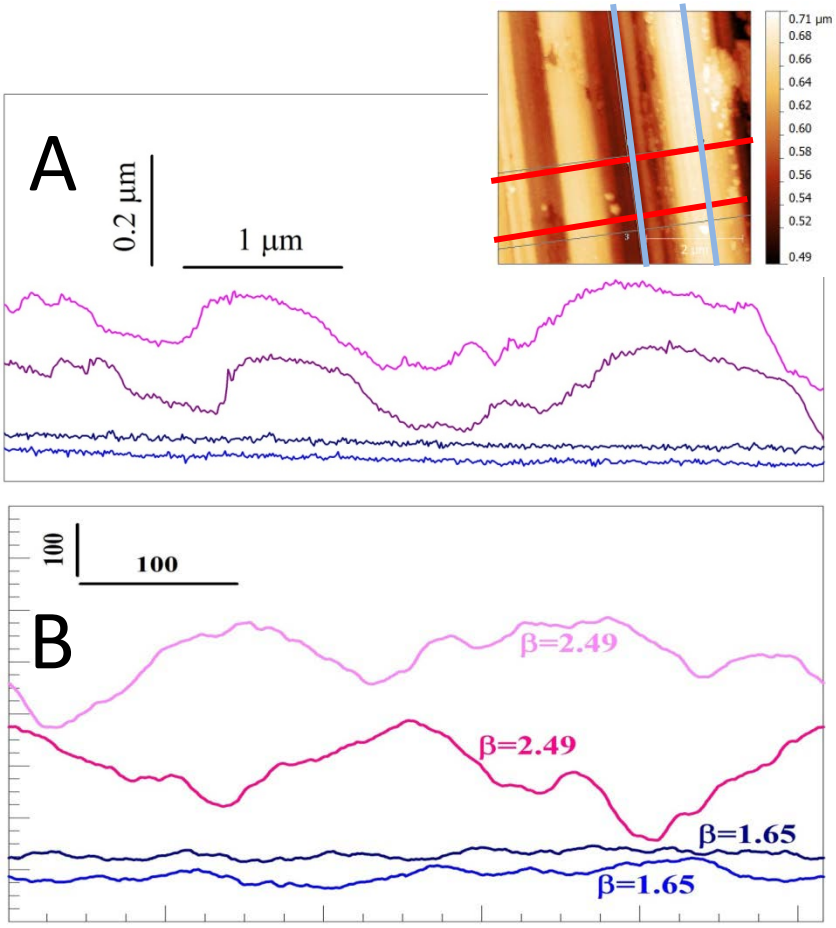

Fig. DR8. A: Examples of four 1D profiles across the KD fault surface on AFM image (inset). The two slip-parallel profiles (blue lines in inset) are significantly smoother than the slip-normal profiles (red line in inset). B: Synthetic profiles with the marked slope (β) in the PSD curve generated with MatLab.

REFERENCES

Hertz, H. On the contact of elastic solids, *J. ReineAngew. Math.***92**, 156 (1881).

Sader, J. E., Chon, J. W. M. & Mulvaney, P. Calibration of rectangular atomic force microscope cantilevers. *Rev. Sci. Instrum.***70**, 3967-3969 (1999).

Sagy, A. & Brodsky, E. E. Geometric and rheological asperities in an exposed fault zone. *J. Geophys. Res.* **114**, B02301 (2009).

Power, W. L., Tullis, T. E. & Weeks, J. D. Roughness and wear during brittle faulting. *J. Geophys. Res.* **93,** 15268-15278 (1988).